



**HAL**  
open science

## **Eu 2+ : A suitable substituent for Pb 2+ in CsPbX 3 perovskite nanocrystals?**

Firoz Alam, K. David Wegner, Stéphanie Pouget, Lucia Amidani, Kristina Kvashnina, Dmitry Aldakov, Peter Reiss

► **To cite this version:**

Firoz Alam, K. David Wegner, Stéphanie Pouget, Lucia Amidani, Kristina Kvashnina, et al.. Eu 2+ : A suitable substituent for Pb 2+ in CsPbX 3 perovskite nanocrystals?. The Journal of Chemical Physics, 2019, 151 (23), pp.231101. 10.1063/1.5126473 . hal-02446917

**HAL Id: hal-02446917**

**<https://hal.science/hal-02446917v1>**

Submitted on 15 Dec 2020

**HAL** is a multi-disciplinary open access archive for the deposit and dissemination of scientific research documents, whether they are published or not. The documents may come from teaching and research institutions in France or abroad, or from public or private research centers.

L'archive ouverte pluridisciplinaire **HAL**, est destinée au dépôt et à la diffusion de documents scientifiques de niveau recherche, publiés ou non, émanant des établissements d'enseignement et de recherche français ou étrangers, des laboratoires publics ou privés.

# Eu<sup>2+</sup>: A suitable substituent for Pb<sup>2+</sup> in CsPbX<sub>3</sub> perovskite nanocrystals?

Cite as: J. Chem. Phys. **151**, 231101 (2019); <https://doi.org/10.1063/1.5126473>

Submitted: 05 September 2019 . Accepted: 21 November 2019 . Published Online: 17 December 2019

Firoz Alam , K. David Wegner , Stephanie Pouget , Lucia Amidani , Kristina Kvashnina , Dmitry Aldakov , and Peter Reiss 

## COLLECTIONS

Paper published as part of the special topic on [Colloidal Quantum Dots](#)

Note: This paper is part of the JCP Special Topic on Colloidal Quantum Dots.



View Online



Export Citation



CrossMark

## ARTICLES YOU MAY BE INTERESTED IN

[Enhanced photoredox activity of CsPbBr<sub>3</sub> nanocrystals by quantitative colloidal ligand exchange](#)

The Journal of Chemical Physics **151**, 204305 (2019); <https://doi.org/10.1063/1.5129261>

[How surface-specific is 2nd-order non-linear spectroscopy?](#)

The Journal of Chemical Physics **151**, 230901 (2019); <https://doi.org/10.1063/1.5129108>

[Quasicubic model for metal halide perovskite nanocrystals](#)

The Journal of Chemical Physics **151**, 234106 (2019); <https://doi.org/10.1063/1.5127528>



Lock-in Amplifiers

Zurich Instruments

Watch the Video

# Eu<sup>2+</sup>: A suitable substituent for Pb<sup>2+</sup> in CsPbX<sub>3</sub> perovskite nanocrystals?

Cite as: J. Chem. Phys. 151, 231101 (2019); doi: 10.1063/1.5126473

Submitted: 5 September 2019 • Accepted: 21 November 2019 •

Published Online: 17 December 2019



View Online



Export Citation



CrossMark

Firoz Alam,<sup>1</sup>  K. David Wegner,<sup>1</sup>  Stephanie Pouget,<sup>2</sup>  Lucia Amidani,<sup>3,4</sup>  Kristina Kvashnina,<sup>3,4</sup>   
Dmitry Aldakov,<sup>1</sup>  and Peter Reiss<sup>1,a)</sup> 

## AFFILIATIONS

<sup>1</sup>University Grenoble Alpes, CEA, CNRS, IRIG, SyMMES, STEP, 38000 Grenoble, France

<sup>2</sup>University Grenoble Alpes, CEA, IRIG, DEPHY, MEM, SGX, 38000 Grenoble, France

<sup>3</sup>The Rossendorf Beamline at ESRF—The European Synchrotron, CS40220, 38043 Grenoble Cedex 9, France

<sup>4</sup>Helmholtz Zentrum Dresden-Rossendorf (HZDR), Institute of Resource Ecology, P.O. Box 510119, 01314 Dresden, Germany

**Note:** This paper is part of the JCP Special Topic on Colloidal Quantum Dots.

**a)** Author to whom correspondence should be addressed: [peter.reiss@cea.fr](mailto:peter.reiss@cea.fr)

## ABSTRACT

Eu<sup>2+</sup> is used to replace toxic Pb<sup>2+</sup> in metal halide perovskite nanocrystals (NCs). The synthesis implies injection of cesium oleate into a solution of europium (II) bromide at an experimentally determined optimum temperature of 130 °C and a reaction time of 60 s. Structural analysis indicates the formation of spherical CsEuBr<sub>3</sub> nanoparticles with a mean size of 43 ± 7 nm. Using EuI<sub>2</sub> instead of EuBr<sub>2</sub> leads to the formation of 18-nm CsI nanoparticles, while EuCl<sub>2</sub> does not show any reaction with cesium oleate forming 80-nm EuCl<sub>2</sub> nanoparticles. The obtained CsEuBr<sub>3</sub> NCs exhibit bright blue emission at 413 nm (FWHM 30 nm) with a room temperature photoluminescence quantum yield of 39%. The emission originates from the Laporte-allowed 4f<sup>7</sup>–4f<sup>6</sup>5d<sup>1</sup> transition of Eu<sup>2+</sup> and shows a PL decay time of 263 ns. The long-term stability of the optical properties is observed, making inorganic lead-free CsEuBr<sub>3</sub> NCs promising deep blue emitters for optoelectronics.

Published under license by AIP Publishing. <https://doi.org/10.1063/1.5126473>

## I. INTRODUCTION

Lead halide perovskites have not only become promising thin-film absorber materials in photovoltaics but also inspire intense research efforts in the form of colloidal semiconductor nanocrystals (NCs).<sup>1–3</sup> Initially, organic-inorganic hybrid perovskite NCs such as methylammonium lead bromide (MAPbBr<sub>3</sub>) were developed, reaching up to unity photoluminescence quantum yield (PLQY) combined with narrow emission linewidths.<sup>4–8</sup> These features make hybrid perovskite NCs very appealing for light-emitting applications; however, due to their high sensitivity to oxygen and moisture, efficient encapsulation strategies are required.<sup>9–11</sup> Fully inorganic lead halide perovskites with the formula ABX<sub>3</sub> (A = Cs<sup>+</sup>, B = Pb<sup>2+</sup>, X = Cl<sup>–</sup>, Br<sup>–</sup>, or I<sup>–</sup>) have already been known since the end of the 19th century,<sup>12</sup> but their perovskite crystal structure and semiconducting nature were not reported until the 1950s.<sup>13</sup> In the form of colloidal

NCs, they show intrinsically higher stability than hybrid perovskites, albeit still lower than conventional II–VI, IV–VI, or III–V semiconductor NCs due to their much stronger ionic characteristic.<sup>2,3,14</sup> While it turned out challenging to stabilize small-sized CsPbX<sub>3</sub> NCs in the strong quantum confinement regime below approximately 5 nm,<sup>2</sup> anion exchange has been shown to be an efficient way to fine tune their optical and electronic properties, with bandgap energies covering the entire visible range.<sup>1,15–17</sup> In the past few years, the high potential of CsPbX<sub>3</sub> NCs for use in diverse optoelectronic applications, such as light-emitting diodes,<sup>18–20</sup> solar cells,<sup>21</sup> and photodetectors,<sup>22–24</sup> has been demonstrated.

Despite these appealing features, the intrinsic toxicity of lead is a roadblock for real-life applications of perovskite NCs, which triggered research on its replacement by less toxic metals.<sup>25</sup> Most of these works focused on elements neighboring lead in the periodic table of elements, namely, tin, bismuth, and antimony.<sup>26</sup> In the

case of tin, one has to consider the much higher oxidation sensitivity of  $\text{Sn}^{2+}$  as compared to  $\text{Pb}^{2+}$  whose divalent state is stabilized by relativistic effects ( $6s^2$  inert electron pair). Jellicoe *et al.* first reported the successful synthesis of  $\text{CsSnBr}_3$  and  $\text{CsSnI}_3$  NCs, however, with low PLQYs (0.14% and 0.06%).<sup>27</sup> Trivalent  $\text{Bi}^{3+}$  is isoelectronic with  $\text{Pb}^{2+}$  and can form 2D layered perovskite NCs of the formula  $\text{A}_3\text{B}_2\text{X}_9$  crystallizing in the trigonal space group P-3m1.<sup>28</sup> The same type of structure can be adopted by the lighter homolog  $\text{Sb}^{3+}$ . The highest reported PLQY for  $\text{Cs}_3\text{Bi}_2\text{Br}_9$  QDs emitting at 410 nm (FWHM 48 nm) is 19.4%<sup>29</sup> and for  $\text{Cs}_3\text{Sb}_2\text{Br}_9$  QDs emitting at the same wavelength (FWHM 41 nm) 46%.<sup>30</sup>

In contrast to these approaches, metal halide perovskite NCs involving rare earth (RE) ions for lead substitution have been essentially unexplored so far, although lanthanides have been used as dopants to modify the emission properties.<sup>31,32</sup> Here, we report the first synthesis and main photophysical properties of colloidal  $\text{CsEuBr}_3$  NCs. Europium has been chosen for its capacity of octahedral coordination in the divalent state and its almost identical ionic radius with  $\text{Pb}^{2+}$  in this hexacoordinated configuration (117 pm/119 pm). The obtained NCs exhibit a PL peak centered at 413 nm, a narrow emission linewidth ( $\leq 30$  nm FWHM), and a PLQY of 39%, which is the highest value reported for Pb-free  $\text{ABX}_3$  NCs.

## II. EXPERIMENTAL

### A. Materials

**Chemicals:** cesium carbonate ( $\text{Cs}_2\text{CO}_3$ , Aldrich, 99.9%), oleic acid (OA, Fisher Chemicals, 70%), 1-octadecene (ODE, Sigma-Aldrich, 90%), oleylamine (OLA, Acros Organics, 80%–90%), europium(III) bromide ( $\text{EuBr}_3$ , Sigma-Aldrich, 99.99%), europium(II) chloride ( $\text{EuCl}_2$ , Sigma-Aldrich, 99.999%), europium(II) iodide ( $\text{EuI}_2$ , Sigma-Aldrich, 99.999%), anhydrous toluene, hexanes, and acetonitrile (all Sigma-Aldrich).

### B. Methods

**Synthesis of Cs-oleate:** The synthesis was adapted from the method reported in Ref. 14. 203.5 mg (0.62 mmol) of  $\text{Cs}_2\text{CO}_3$ , 10 ml of ODE, and 0.625 ml of dried OA (1.97 mmol) were loaded into a 50 ml three-neck flask equipped with a condenser. The reaction mixture was continuously stirred and degassed for 1 h at 120 °C under primary vacuum using a Schlenk line for the removal of oxygen and moisture. Later, the system was switched to an argon atmosphere and the temperature was increased to 150 °C to get a clear solution of Cs-oleate. Cs-oleate solidifies at room temperature, and it must be heated to 100 °C before injection.

**Synthesis of  $\text{CsEuBr}_3$  NCs:** Colloidal  $\text{CsEuBr}_3$  NCs were synthesized using a hot-injection method. Typically, within a glove-box 58.6 mg (0.188 mmol) of europium bromide and 5 ml of ODE were loaded into a 50 ml three-neck flask. Outside the glove-box, the flask was connected to a condenser and degassed at 120 °C for 60 min using a Schlenk line. After backfilling with argon, dried OLA and OA (0.5 ml each) were injected into the reaction mixture. Within 15 min, a clear colorless solution was obtained and the reaction temperature was increased to 130 °C. The Cs-oleate solution (0.4 ml of the 0.12 M stock solution, preheated to 100 °C) was swiftly injected, and 1 min later, the reaction was cooled down by immersion in an

ice/water bath. The  $\text{CsEuBr}_3$  NCs were purified by adding 1.5 ml of hexanes followed by centrifugation at 1000 rpm for 5 min. The supernatant was discarded, and a second cycle of purification was carried out by adding 1.5 ml of anhydrous acetonitrile to the precipitate followed by vortexing and centrifugation as before. Finally, the precipitated NCs were redispersed in a nonpolar solvent such as hexanes or toluene for further analysis.

**Synthesis attempts for  $\text{CsEuCl}_3$  and  $\text{CsEuI}_3$  NCs:** In the above-described reaction  $\text{EuBr}_2$  was replaced by  $\text{EuCl}_2$  or  $\text{EuI}_2$ , respectively. In the former case, higher temperatures (170–180 °C) and longer times (2 h) were required for the complexation of the europium salt prior to Cs-oleate injection.

## C. Characterization

### 1. Powder X-ray diffraction

Powder X-ray diffraction was performed using a Panalytical X'Pert powder diffractometer equipped with a copper anode ( $\lambda_{\text{K}\alpha 1} = 1.5406 \text{ \AA}$  and  $\lambda_{\text{K}\alpha 2} = 1.5444 \text{ \AA}$ ) and an X'Celerator 1D detector. It was configured in Bragg-Brentano geometry, with a variable divergence slit on the primary beam path and a set of antiscattering slits positioned before and after the sample. Axial divergence was limited by 0.02 rad Soller slits. The XRD samples were prepared in a glove box by drop-casting a concentrated NC dispersion in hexane on a disoriented silicon substrate and sealed with a double layer of airtight Kapton<sup>®</sup> foils within the sample holder.

### 2. XANES measurements on ID26 at ESRF

Eu  $L_3$ -edge X-ray absorption near edge structure (XANES) in High-Energy Resolution Fluorescence Detection (HERFD) mode was acquired on the ID26 beamline of the ESRF.<sup>33</sup> The incident energy was selected by a Si(311) double crystal monochromator. The footprint of the beam on the sample surface, oriented at 45° to the incident beam direction, was 600  $\mu\text{m}$  horizontal times 150  $\mu\text{m}$  vertical. The HERFD XANES at the Eu  $L_3$  edge was collected using an X-ray emission spectrometer in Rowland geometry equipped with four spherically bent Ge(333) crystal analyzers. The spectrometer was moved to the energy of the maximum of the Eu  $L\alpha_1$  characteristic fluorescence line in order to collect only emitted photons in a 0.8 eV energy bandwidth around the maximum of the Eu  $L\alpha_1$ . Collecting the emitted photons on a bandwidth smaller than the core-hole lifetime broadening results in a sharpening of the XANES features compared to the conventional fluorescence detected XANES, which integrates the full characteristic line.<sup>34</sup> The overall (incoming and emitted) energy resolution was 0.8 eV. All samples were measured in a liquid He cryostat kept at 20 K in order to minimize the X-ray beam damage and the contact with air.

We carefully checked for X-ray beam damage on all samples by acquiring fast XANES of the edge region. On sensitive samples, we adapted the thickness of Al attenuators and the scan time per spectrum to acquire HERFD XANES with minimal X-ray damage and we measured single XANES on several sample spots to have the desired statistics.

### 3. SEM and EDX

A ZEISS Ultra 55+ scanning electron microscope equipped with an EDX probe (acceleration tension: 20 keV and distance

sample/electron source: 7 nm) was used to obtain the images of the NCs and to determine the elemental composition. For sample preparation, a concentrated colloidal solution of CsEuBr<sub>3</sub> NCs in chloroform is drop cast on a cleaned silicon substrate.

#### 4. Transmission electron microscopy

Conventional transmission electron microscopy (TEM) images were acquired on a JEOL 3010 LaB6 microscope equipped with a thermionic gun at 300 kV accelerating voltage. The samples were prepared by drop-casting diluted NC solution onto 200-mesh carbon-coated copper grids. STEM-HAADF images were recorded on an aberration corrected FEI Titan Themis<sup>3</sup> microscope using an acceleration voltage of 200 kV.

#### 5. UV-visible absorption spectroscopy

UV-vis spectroscopy was performed with a Hewlett Packard 8452A single beam spectrophotometer operating in the wavelength range of 190–820 nm and using a diode array for detection. The samples were prepared by diluting the NC dispersions in toluene or hexane in quartz cuvettes with a path length of 4 mm or 1 cm. The background was acquired using the pure solvent.

#### 6. Steady-state and time-resolved photoluminescence

Photoluminescence spectra were recorded using a modular Fluorolog FL3-22 system from Horiba-Jobin Yvon equipped with a double grating excitation monochromator and an iHR320 imaging spectrometer. A Hamamatsu R928P photomultiplier and quartz cuvettes with a path length of 1 cm were used for the measurement. For the PL measurements, the concentration of the samples was adjusted to an absorbance around 0.1 at the excitation wavelength.

PL lifetimes of the NCs were obtained using a NanoLED pulsed source from Horiba (emission wavelength: 360 nm and repetition rate: 1 MHz). The output signal was controlled and analyzed with Data Station (v2.7) and Decay Analysis (v6.8) software from Horiba Scientist. The quantum yield measurements were performed at room temperature using an integration sphere, Hamamatsu Quantaaurus-QY Absolute PL quantum yield spectrometer C11347-11.

### III. RESULTS AND DISCUSSION

Alkali halide compounds of divalent RE ions are generally synthesized by high temperature reactions between stoichiometric amounts of the RE halide and the alkali halide.<sup>35</sup> In the case of europium(II) and cesium, the formation of perovskite-type ternary compounds of the formula CsEuX<sub>3</sub> (X = Cl, Br) was observed, while ARE<sub>2</sub>X<sub>5</sub> compounds are obtained for smaller alkaline ions (Rb, K). In attempts to develop synthetic methods for nanoparticles of CsEuX<sub>3</sub>, major challenges are related to the low solubility and high oxidation sensitivity of europium(II) halides used as precursors. As a starting point, the well-established hot-injection method reported for CsPbBr<sub>3</sub> NCs was applied,<sup>14</sup> using EuBr<sub>2</sub> instead of PbBr<sub>2</sub>. In brief, a cesium oleate solution was quickly injected into a hot mixture of EuBr<sub>2</sub>, oleic acid (OA), and oleylamine (OLA) in 1-octadecene (ODE). For an optimized reaction temperature of 130 °C and a reaction time of 60 s (*vide infra*), CsEuBr<sub>3</sub> NCs of approximately spherical shape with a mean size of 43 ± 7 nm were obtained

as revealed by SEM and TEM analyses shown in Fig. 1. Shorter reaction times (5–10 s) did not give access to smaller NCs but yielded ill-defined mixtures of larger particles and sheet-like structures (cf. Fig. S1). In the high-resolution TEM image [Fig. 1(b)], lattice planes can be identified throughout the entire particle, confirming the high crystallinity of the obtained NCs, which are sensitive to beam damage as visible by the darker areas in the image. The observed lattice spacing of 0.295 nm corresponds to (004) planes in CsEuBr<sub>3</sub> (ICDD card No. 04-014-8774)<sup>36</sup> and cannot be found in related secondary phases such as CsBr or EuBr<sub>2</sub>. EDX analyses resulted in a Cs:Eu ratio of 1:0.92, i.e., close to the expected 1:1 ratio in CsEuBr<sub>3</sub>, indicating that possible other phases such as Cs<sub>2</sub>EuBr<sub>4</sub> or Cs<sub>4</sub>EuBr<sub>6</sub> do not form or are minority phases.<sup>37</sup> We note, however, a slightly elevated Br ratio of 3.86, which we attribute to remaining bromide after purification and/or oleylammonium bromide passivating the surface.

The structure of CsEuBr<sub>3</sub> single crystals has been reported to correspond to a distorted 3D perovskite structure, with an  $a^- a^- c^+$  tilting scheme of the EuBr<sub>6</sub> octahedra.<sup>36</sup> It is isotypic to GdFeO<sub>3</sub> and crystallizes in the orthorhombic space group *Pbnm*. The powder X-ray data of the synthesized CsEuBr<sub>3</sub> NCs [Figs. 2(a) and 2(b)] reveal prominent peaks similar to the diffraction pattern of CsBr as well as a number of additional peaks characteristic of the formation of the ternary structure. However, the diffraction pattern does not match the powder XRD data reported for ground CsEuBr<sub>3</sub> single crystals.<sup>38</sup> Analysis of the XRD peak linewidth does not reveal the presence of different sets of peaks and therefore does not give any indication that several crystalline phases coexist. We emphasize that the obtained XRD data cannot be assigned to Eu<sup>2+</sup>-doped CsBr nanocrystals, which exhibit essentially the crystal structure of CsBr with few very low intensity additional peaks in the lower 2 theta angle range.<sup>32,38</sup> The data were also compared with several other related structures, namely, CsPbBr<sub>3</sub> nanocrystals as well as bulk EuBr<sub>2</sub>, Cs<sub>2</sub>PbBr<sub>4</sub>, and Cs<sub>4</sub>PbBr<sub>6</sub>, yet none of these phases fits the experimental data. Several reasons can be at the origin of the observed structural differences. First, structural modifications occurring during the measurement could be eventually expected in view of the high sensitivity against radiation damage observed in Eu<sup>2+</sup>-doped CsBr used in X-ray radiography based on photo-stimulated luminescence (PSL).<sup>39</sup> However, by examining a series of diffractograms recorded in successive scans, we can exclude this effect being responsible for the observed structural features. Second, AREX<sub>3</sub> compounds are well-known to form several hettotypes

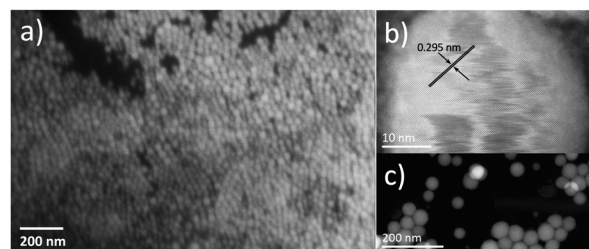
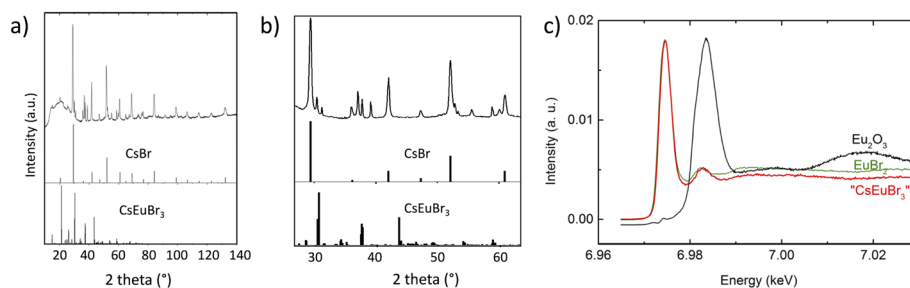


FIG. 1. (a) SEM image of the obtained CsEuBr<sub>3</sub> NCs (mean size 43 ± 7 nm), (b) high-resolution, and (c) low-resolution STEM-HAADF images.



**FIG. 2.** (a) Powder X-ray diffractogram of CsEuBr<sub>3</sub> NCs. The broad feature in the 10°–30° range originates from two Kapton foils used to protect the sample against oxidation during the measurement (cf. Fig. S2). For comparison, the diffraction patterns of bulk CsBr (ICCD No. 00-005-0588) and CsEuBr<sub>3</sub> (ICCD No. 04-014-8774) are also given. (b) Zoomed-in image of the 30°–60° 2 theta range. (c) HERFD XANES spectrum at the Eu L<sub>3</sub> edge of CsEuBr<sub>3</sub> NCs compared with the reference systems Eu<sub>2</sub>O<sub>3</sub> and EuBr<sub>2</sub>.

arising from octahedral tilting and to frequently undergo phase transitions, both of which can contribute to the observed structural differences.<sup>35</sup> Third, a possible formation mechanism could start with CsBr host nanoparticles, in which Eu<sup>2+</sup> ions are integrated followed by the transformation to a perovskite-like CsEuBr<sub>3</sub> structure. Interestingly, in the case of M<sup>2+</sup>-doped bulk cesium halides, the formation of perovskite-type domains has been postulated and demonstrated. In particular, Eu<sup>2+</sup>-doped CsBr is characterized by charge-compensating cation vacancies ( $v_c$ ) and a fast aggregation of Eu<sup>2+</sup>- $v_c$  dimers at room temperature.<sup>40</sup> The formation of the perovskite-type unit cell has been explained by means of Nikl's mechanism for CsPbCl<sub>3</sub>.<sup>41</sup> This mechanism implies local structural disorder due to ionic mobility. A similar mechanism has been proposed to occur in the case of CsEuBr<sub>3</sub>.<sup>40</sup> Therefore, local structural disorder occurring during the formation of the perovskite-like CsEuBr<sub>3</sub> structure is a plausible reason for the observed structural features.

X-ray absorption near edge structure (XANES) spectroscopy at the Eu L<sub>3</sub> edge was used to identify the oxidation state of europium in the obtained NCs. XANES spectroscopy is one of the most powerful methods for the investigation of the electronic structure. Electrons in the X-ray absorption process are excited to unoccupied levels and give information about the chemical state. A chemical shift in the absorption edge can therefore be assigned to a certain oxidation state. Better energy resolution of the XANES spectra can be obtained using the high energy resolution fluorescence detection (HERFD) mode, where an X-ray emission spectrometer is employed for data collection. Figure 2(c) shows the HERFD XANES spectra at the Eu L<sub>3</sub> edge of CsEuBr<sub>3</sub> NCs compared to two reference systems (Eu<sub>2</sub>O<sub>3</sub> and EuBr<sub>2</sub>) with Eu(III) and Eu(II) oxidation states, respectively. The position of the main peak in the HERFD XANES spectrum of CsEuBr<sub>3</sub> NCs clearly demonstrates the predominance of the Eu(II) oxidation state, based on the good correspondence with the EuBr<sub>2</sub> reference. The exact contribution of the different chemical states in the Eu L<sub>3</sub> HERFD XANES data depicted in Fig. 2(c) was estimated using the ITFA program.<sup>42</sup> The results (reported in the supplementary material) indicate that the spectrum of CsEuBr<sub>3</sub> NCs contains 99% of Eu(II) (with an estimated root mean square error of less than 1%).

An interesting feature of the obtained NCs is their strong luminescence in the deep blue range. In the PL spectrum of CsEuBr<sub>3</sub> NCs

[Fig. 3(a)], an emission peak centered at 413 nm with a linewidth of 30 nm (FWHM) is observed whose position is independent of the excitation wavelength (330 or 360 nm). This peak is blue shifted compared to Eu<sup>2+</sup>-doped bulk CsBr or CsBr NCs (440 nm) and to CsEuBr<sub>3</sub> single crystals (450 nm).<sup>32,38,43</sup> In the former case, no perovskite structure is formed, but Eu<sup>2+</sup> occupies cesium positions, which leads to the creation of Cs<sup>+</sup> vacancies in their immediate surrounding for charge compensation.<sup>37</sup> The observed hypsochromic shift with respect to the single crystal data indicates differences within the coordination sphere of the Eu<sup>2+</sup> ion in CsEuBr<sub>3</sub> NCs, as already suggested by the X-ray data. For samples kept under inert atmosphere, no PL emission signals in the 600–700 nm range characteristic of the 5D<sub>0</sub>–7F<sub>J</sub> transitions of Eu<sup>3+</sup> ions were detected,<sup>44</sup> even when using longer excitation wavelengths. This is an indirect proof that no oxidation took place. Moreover, also after storing the samples for one month in toluene or hexanes, no change of the PL spectra occurred (Fig. S6), demonstrating the long-term stability of the obtained CsEuBr<sub>3</sub> NCs. In the UV-vis absorption spectrum [Fig. 3(c)] for strongly diluted samples, an absorption band comprising several features and peaking at 263 nm becomes visible, attributed to the 4f<sup>7</sup>–4f<sup>6</sup>5d<sup>1</sup> transition.<sup>45</sup> In contrast to the absorption spectra of Eu<sup>2+</sup> containing phosphors prepared in alkali halide melts,<sup>46</sup> no separation into two bands is observed. In particular, no second absorption band in the range of 300–350 nm due to the splitting of the Eu<sup>2+</sup> 5d orbitals by the crystal field is visible. In the 300–800 nm range, the absorption spectrum is featureless [blue curve in Fig. 3(c)], while the photoluminescence excitation (PLE) spectrum exhibits two small humps at around 320 and 355 nm (red curve).

The PL decay curve obtained in time-resolved measurements [Fig. 3(d)] was fitted with a triexponential function, resulting in lifetimes of  $\tau_1$  9.7 ns ( $A_1$  1.9),  $\tau_2$  124.5 ns ( $A_2$  35.7), and  $\tau_3$  296.0 ns ( $A_3$  62.5), yielding an average lifetime (intensity weighted) of 262.6 ns. As the underlying transition is Laporte-allowed, the lifetime is several orders of magnitude lower than that of well-known emitters involving Eu<sup>3+</sup> ions ( $\tau$  in the millisecond range). The PLQY of the as-synthesized CsEuBr<sub>3</sub> NCs, measured at room temperature using an integration sphere, accounts for 39%. Except for one example (NCs of the 2D perovskite Cs<sub>3</sub>Sb<sub>2</sub>Br<sub>9</sub> emitting at 410 nm with a PLQY of 46%),<sup>30</sup> this is the highest value reported for lead-free metal halide perovskite NCs luminescing in the deep blue range.<sup>47</sup>

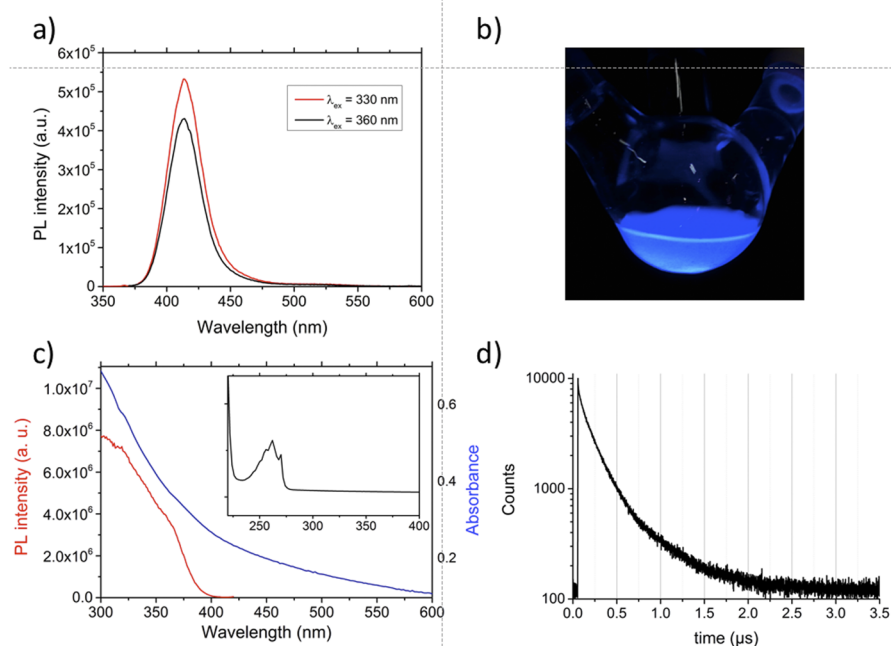


**FIG. 3.** (a) PL spectra of CsEuBr<sub>3</sub> NCs using two different excitation wavelengths in hexanes. The PL peak is centered at 413 nm (FWHM 30 nm). (b) Photograph of the colloidal solution under UV light (360 nm). (c) UV-vis absorption spectrum (blue) and PLE spectrum (red,  $\lambda_{em} = 425$  nm). Inset: absorption spectrum of a strongly diluted colloidal solution. (d) Time-resolved PL spectrum.

indicating that CsEuBr<sub>3</sub> NCs are promising toxic heavy metal-free emitters for optoelectronic applications.

While for lead-based perovskite NCs, the variation of the reaction temperature is used to tune the NC size, here, this parameter had a critical influence on the optical properties of the product. At high temperatures (>130 °C), either no emission was detectable (180 °C) or partial oxidation of Eu<sup>2+</sup> took place (150 °C), visible by the appearance of PL bands characteristic of Eu<sup>3+</sup> in the 600–700 nm range (cf. Fig. S4). As all reactions were carried out under strict air- and moisture-free conditions, oxidation could arise from side reactions of the used surface ligands, such as, for example, amide formation<sup>48</sup> or ketonization,<sup>49</sup> leading to the *in situ* formation of minute amounts of water. Degradation of the optical properties continues to progress within a few days of storage. At lower reaction temperatures (e.g., 110 °C), only partial conversion of the precursors and low reaction yields are observed, combined with limited stability (cf. Fig. S5). 130 °C turned out to be an optimum value, leading to the long-term stability (at least 1 month) of the optical properties, both in terms of spectral shape and PLQY (Fig. S6).

To check the influence of the halide ion, additional experiments were conducted using EuCl<sub>2</sub> and EuI<sub>2</sub> as precursors. In the former case, EuCl<sub>2</sub> could not be solubilized in ODE containing a mixture of OA and OLA, even when higher temperatures (up to 180 °C) and longer reaction times (up to two days) were applied. EuCl<sub>2</sub> has a much higher bond dissociation energy (414 kJ/mol) as compared to EuBr<sub>2</sub> (347 kJ/mol) and PbCl<sub>2</sub> (304 kJ/mol) or PbBr<sub>2</sub> (260 kJ/mol).<sup>50</sup> In consequence, no reaction with Cs-oleate took place under the used experimental conditions: the isolated precipitate was identified by means of powder X-ray diffraction as EuCl<sub>2</sub> nanoparticles having a crystallite size of around 80 nm (Fig. S7). In contrast, EuI<sub>2</sub>

(bond dissociation energy: 272 kJ/mol) could be easily solubilized at 130 °C in the presence of OLA and OA. However, upon Cs-oleate injection, no visible change occurred, and only for longer reaction times (>15 min), a white precipitate could be isolated. The product was identified using XRD as 18-nm CsI nanoparticles of low size dispersion (cf. Fig. S8).

#### IV. CONCLUSION

CsEuBr<sub>3</sub> NCs were synthesized using a hot-injection method at 130 °C. They exhibit a narrow PL peak at 413 nm with a PLQY of 39%, which represents the highest reported value for lead-free ABX<sub>3</sub> perovskite NCs. No change in their optical properties was observed over one month when exposure to air and moisture was avoided. These features make CsEuBr<sub>3</sub> NCs promising candidates for optoelectronic applications, such as, for example, UV-to-blue color converters in LEDs.<sup>47</sup> Nonetheless, unlike lead-based perovskite NCs, their luminescence cannot be varied in a wide spectral range. In CsPbX<sub>3</sub> NCs, excitonic emission takes place between band edge states constituted of Pb<sup>2+</sup> and X<sup>-</sup> electronic orbitals and the position of these levels can be tuned by changing the size of the particles (via the quantum confinement effect) or the nature of the halide.<sup>25</sup> In contrast, the PL emission of CsEuBr<sub>3</sub> NCs results from the intrinsic  $4f^7-4f^65d^1$  transition of Eu<sup>2+</sup> whose energy cannot be tuned using similar approaches but is influenced by the coordination sphere of the europium ion. Nevertheless, other emission ranges could be accessed by using different types of REs, e.g., Sm<sup>2+</sup>. As such, this first example of RE halide perovskite NCs can serve as a basis for the development of related systems involving the use of different lanthanide ions and/or different halides. To overcome the solubility issues of RE<sup>2+</sup> halides, synthetic schemes

allowing for the separate introduction of the three individual constituents of  $ABX_3$ , by decoupling the B and X precursors, will be particularly useful in this context. This has recently been achieved by using, for example, benzoyl halide or molecular halogen as the X source.<sup>51,52</sup>

## SUPPLEMENTARY MATERIAL

See the [supplementary material](#) for additional XRD, SEM, and photoluminescence data and for the description of the ITFA method used for XANES data analysis.

## ACKNOWLEDGMENTS

The authors acknowledge the French Research Agency ANR for financial support (Grant Nos. SuperSansPlomb ANR-15-CE05-0023-01 and PERSIL ANR-16-CE05-0019-02). K.D.W. acknowledges the LABEX Serenade (Grant No. ANR 11-LABX-0064) for his post-doctoral funding. F.A. acknowledges support from the PHC program MERLION financing an exchange with Nanyang Technical University Singapore. Hanako Okuna is thanked for TEM imaging. The authors gratefully acknowledge the help of Tim Bohdan at the ID26 beamline of ESRF during the HERFD XANES measurements. L.A. and K.K. acknowledge support from the European Research Council under ERC Grant No. N759696.

## REFERENCES

- J. Shamsi, A. S. Urban, M. Imran, L. De Trizio, and L. Manna, "Metal halide perovskite nanocrystals: Synthesis, post-synthesis modifications, and their optical properties," *Chem. Rev.* **119**(5), 3296–3348 (2019).
- M. V. Kovalenko, L. Protesescu, and M. I. Bodnarchuk, "Properties and potential optoelectronic applications of lead halide perovskite nanocrystals," *Science* **358**(6364), 745–750 (2017).
- Q. A. Akkerman, G. Rainò, M. V. Kovalenko, and L. Manna, "Genesis, challenges and opportunities for colloidal lead halide perovskite nanocrystals," *Nat. Mater.* **17**(5), 394–405 (2018).
- L. C. Schmidt, A. Pertegás, S. González-Carrero, O. Malinkiewicz, S. Agouram, G. Mínguez Espallargas, H. J. Bolink, R. E. Galian, and J. Pérez-Prieto, "Nontemplate synthesis of  $CH_3NH_3PbBr_3$  perovskite nanoparticles," *J. Am. Chem. Soc.* **136**(3), 850–853 (2014).
- S. Gonzalez-Carrero, R. E. Galian, and J. Perez-Prieto, "Maximizing the emissive properties of  $CH_3NH_3PbBr_3$  perovskite nanoparticles," *J. Mater. Chem. A* **3**(17), 9187–9193 (2015).
- S. Gonzalez-Carrero, L. Francés-Soriano, M. González-Béjar, S. Agouram, R. E. Galian, and J. Pérez-Prieto, "The luminescence of  $CH_3NH_3PbBr_3$  perovskite nanoparticles crests the summit and their photostability under wet conditions is enhanced," *Small* **12**(38), 5245–5250 (2016).
- F. Zhang, H. Zhong, C. Chen, X.-g. Wu, X. Hu, H. Huang, J. Han, B. Zou, and Y. Dong, "Brightly luminescent and color-tunable colloidal  $CH_3NH_3PbX_3$  (X = Br, I, Cl) quantum dots: Potential alternatives for display technology," *ACS Nano* **9**(4), 4533–4542 (2015).
- H. Huang, J. Raith, S. V. Kershaw, S. Kalytchuk, O. Tomanec, L. Jing, A. S. Susha, R. Zboril, and A. L. Rogach, "Growth mechanism of strongly emitting  $CH_3NH_3PbBr_3$  perovskite nanocrystals with a tunable bandgap," *Nat. Commun.* **8**(1), 996 (2017).
- W. Deng, X. Xu, X. Zhang, Y. Zhang, X. Jin, L. Wang, S. T. Lee, and J. Jie, "Organometal halide perovskite quantum dot light-emitting diodes," *Adv. Funct. Mater.* **26**(26), 4797–4802 (2016).
- Y. Ling, Z. Yuan, Y. Tian, X. Wang, J. C. Wang, Y. Xin, K. Hanson, B. Ma, and H. Gao, "Bright light-emitting diodes based on organometal halide perovskite nanoplatelets," *Adv. Mater.* **28**(2), 305–311 (2016).
- H. Huang, M. I. Bodnarchuk, S. V. Kershaw, M. V. Kovalenko, and A. L. Rogach, "Lead halide perovskite nanocrystals in the research spotlight: Stability and defect tolerance," *ACS Energy Lett.* **2**(9), 2071–2083 (2017).
- H. L. Wells, "Über die Cäsium- und Kalium-Bleihalogenide," *Z. Anorg. Chem.* **3**(1), 195–210 (1893).
- C. K. Möller, "Crystal structure and photoconductivity of caesium plumbahalides," *Nature* **182**, 1436 (1958).
- L. Protesescu, S. Yakunin, M. I. Bodnarchuk, F. Krieg, R. Caputo, C. H. Hendon, R. X. Yang, A. Walsh, and M. V. Kovalenko, "Nanocrystals of cesium lead halide perovskites ( $CsPbX_3$ , X = Cl, Br, and I): Novel optoelectronic materials showing bright emission with wide color gamut," *Nano Lett.* **15**(6), 3692–3696 (2015).
- D. M. Jang, K. Park, D. H. Kim, J. Park, F. Shojaei, H. S. Kang, J.-P. Ahn, J. W. Lee, and J. K. Song, "Reversible halide exchange reaction of organometal trihalide perovskite colloidal nanocrystals for full-range band gap tuning," *Nano Lett.* **15**(8), 5191–5199 (2015).
- Q. A. Akkerman, V. D'Innocenzo, S. Accornero, A. Scarpellini, A. Petrozza, M. Prato, and L. Manna, "Tuning the optical properties of cesium lead halide perovskite nanocrystals by anion exchange reactions," *J. Am. Chem. Soc.* **137**, 10276–10281 (2015).
- G. Nedelcu, L. Protesescu, S. Yakunin, M. I. Bodnarchuk, M. J. Grotevent, and M. V. Kovalenko, "Fast anion-exchange in highly luminescent nanocrystals of cesium lead halide perovskites ( $CsPbX_3$ , X = Cl, Br, I)," *Nano Lett.* **15**(8), 5635–5640 (2015).
- S. G. R. Bade, J. Li, X. Shan, Y. Ling, Y. Tian, T. Dilbeck, T. Besara, T. Geske, H. Gao, B. Ma, K. Hanson, T. Siegrist, C. Xu, and Z. Yu, "Fully printed halide perovskite light-emitting diodes with silver nanowire electrodes," *ACS Nano* **10**(2), 1795–1801 (2016).
- M. F. Aygüler, M. D. Weber, B. M. D. Puscher, D. D. Medina, P. Docampo, and R. D. Costa, "Light-emitting electrochemical cells based on hybrid lead halide perovskite nanoparticles," *J. Phys. Chem. C* **119**(21), 12047–12054 (2015).
- S. Colella, M. Mazzeo, A. Rizzo, G. Gigli, and A. Listorti, "The bright side of perovskites," *J. Phys. Chem. Lett.* **7**(21), 4322–4334 (2016).
- A. Swarnkar, A. R. Marshall, E. M. Sanehira, B. D. Chernomordik, D. T. Moore, J. A. Christians, T. Chakrabarti, and J. M. Luther, "Quantum dot-induced phase stabilization of  $\alpha$ - $CsPbI_3$  perovskite for high-efficiency photovoltaics," *Science* **354**(6308), 92–95 (2016).
- P. Ramasamy, D.-H. Lim, B. Kim, S.-H. Lee, M.-S. Lee, and J.-S. Lee, "All-inorganic cesium lead halide perovskite nanocrystals for photodetector applications," *Chem. Commun.* **52**(10), 2067–2070 (2016).
- L. Lv, Y. Xu, H. Fang, W. Luo, F. Xu, L. Liu, B. Wang, X. Zhang, D. Yang, W. Hu, and A. Dong, "Generalized colloidal synthesis of high-quality, two-dimensional cesium lead halide perovskite nanosheets and their applications in photodetectors," *Nanoscale* **8**(28), 13589–13596 (2016).
- M. I. Saidaminov, M. A. Haque, M. Savoie, A. L. Abdelhady, N. Cho, I. Dursun, U. Buttner, E. Alarousu, T. Wu, and O. M. Bakr, "Perovskite photodetectors operating in both narrowband and broadband regimes," *Adv. Mater.* **28**(37), 8144–8149 (2016).
- D. Aldakov and P. Reiss, "Safer-by-design fluorescent nanocrystals: Metal halide perovskites vs semiconductor quantum dots," *J. Phys. Chem. C* **123**(20), 12527–12541 (2019).
- J. Sun, J. Yang, J. I. Lee, J. H. Cho, and M. S. Kang, "Lead-free perovskite nanocrystals for light-emitting devices," *J. Phys. Chem. Lett.* **9**(7), 1573–1583 (2018).
- T. C. Jellicoe, J. M. Richter, H. F. J. Glass, M. Tabachnyk, R. Brady, S. E. Dutton, A. Rao, R. H. Friend, D. Credgington, N. C. Greenham, and M. L. Böhm, "Synthesis and optical properties of lead-free cesium tin halide perovskite nanocrystals," *J. Am. Chem. Soc.* **138**(9), 2941–2944 (2016).
- M. Leng, Z. Chen, Y. Yang, Z. Li, K. Zeng, K. Li, G. Niu, Y. He, Q. Zhou, and J. Tang, "Lead-free, blue emitting bismuth halide perovskite quantum dots," *Angew. Chem., Int. Ed.* **55**(48), 15012–15016 (2016).
- M. Leng, Y. Yang, K. Zeng, Z. Chen, Z. Tan, S. Li, J. Li, B. Xu, D. Li, M. P. Hautzinger, Y. Fu, T. Zhai, L. Xu, G. Niu, S. Jin, and J. Tang, "All-inorganic

bismuth-based perovskite quantum dots with bright blue photoluminescence and excellent stability,” *Adv. Funct. Mater.* **28**(1), 1704446 (2018).

- <sup>30</sup>J. Zhang, Y. Yang, H. Deng, U. Farooq, X. Yang, J. Khan, J. Tang, and H. Song, “High quantum yield blue emission from lead-free inorganic antimony halide perovskite colloidal quantum dots,” *ACS Nano* **11**(9), 9294–9302 (2017).
- <sup>31</sup>G. Pan, X. Bai, D. Yang, X. Chen, P. Jing, S. Qu, L. Zhang, D. Zhou, J. Zhu, W. Xu, B. Dong, and H. Song, “Doping lanthanide into perovskite nanocrystals: Highly improved and expanded optical properties,” *Nano Lett.* **17**(12), 8005–8011 (2017).
- <sup>32</sup>Z. Yang, Z. Jiang, X. Liu, X. Zhou, J. Zhang, and W. Li, “Bright blue light-emitting doped cesium bromide nanocrystals: Alternatives of lead-free perovskite nanocrystals for white LEDs,” *Adv. Opt. Mater.* **7**(10), 1900108 (2019).
- <sup>33</sup>C. Gauthier, V. A. Solé, R. Signorato, J. Goulon, and E. Moguiline, “The ESRF beamline ID26: X-ray absorption on ultra dilute sample,” *J. Synchrotron Radiat.* **6**(3), 164–166 (1999).
- <sup>34</sup>P. Glatzel, T.-C. Weng, K. Kvashnina, J. Swarbrick, M. Sikora, E. Gallo, N. Smolentsev, and R. A. Mori, “Reflections on hard X-ray photon-in/photon-out spectroscopy for electronic structure studies,” *J. Electron Spectrosc. Relat. Phenom.* **188**, 17–25 (2013).
- <sup>35</sup>G. Meyer, “The synthesis and structures of complex rare-earth halides,” *Prog. Solid State Chem.* **14**(3), 141–219 (1982).
- <sup>36</sup>H. Ehrenberg, H. Fuess, S. Hesse, J. Zimmermann, H. von Seggern, and M. Knapp, “Structures of CsEuBr<sub>3</sub> and its degradation product Cs<sub>2</sub>EuBr<sub>5</sub>·10H<sub>2</sub>O,” *Acta Crystallogr., Sect. B: Struct. Sci.* **63**(2), 201–204 (2007).
- <sup>37</sup>Y. Wu, D. Han, B. C. Chakoumakos, H. Shi, S. Chen, M.-H. Du, I. Greeley, M. Loyd, D. J. Rutstrom, L. Stand, M. Koschan, and C. L. Melcher, “Zero-dimensional Cs<sub>4</sub>EuX<sub>6</sub> (X = Br, I) all-inorganic perovskite single crystals for gamma-ray spectroscopy,” *J. Mater. Chem. C* **6**(25), 6647–6655 (2018).
- <sup>38</sup>S. Hesse, J. Zimmermann, H. V. Seggern, H. Ehrenberg, H. Fuess, C. Fasel, and R. Riedel, “CsEuBr<sub>3</sub>: Crystal structure and its role in the photostimulation of CsBr:Eu<sup>2+</sup>,” *J. Appl. Phys.* **100**(8), 083506 (2006).
- <sup>39</sup>J. Zimmermann, S. Hesse, H. von Seggern, M. Fuchs, and W. Knüpf, “Radiation hardness of CsBr:Eu<sup>2+</sup>,” *J. Lumin.* **114**(1), 24–30 (2005).
- <sup>40</sup>P. Hackenschmied, G. Schierning, M. Batentschuk, and A. Winnacker, “Precipitation-induced photostimulated luminescence in CsBr:Eu<sup>2+</sup>,” *J. Appl. Phys.* **93**(9), 5109–5112 (2003).
- <sup>41</sup>M. Nikl, K. Nitsch, K. Polak, G. P. Pazzi, P. Fabeni, D. S. Citrin, and M. Gurioli, “Optical properties of the Pb<sup>2+</sup>-based aggregated phase in a CsCl host crystal: Quantum-confinement effects,” *Phys. Rev. B* **51**(8), 5192–5199 (1995).
- <sup>42</sup>A. Rossberg, T. Reich, and G. Bernhard, “Complexation of uranium(vi) with protocatechuic acid-application of iterative transformation factor analysis to EXAFS spectroscopy,” *Anal. Bioanal. Chem.* **376**(5), 631–638 (2003).
- <sup>43</sup>P. Hackenschmied, G. Zeitler, M. Batentschuk, A. Winnacker, B. Schmitt, M. Fuchs, E. Hell, and W. Knüpf, “Storage performance of X-ray irradiated doped CsBr,” *Nucl. Instrum. Methods Phys. Res., Sect. B* **191**(1), 163–167 (2002).
- <sup>44</sup>U. T. D. Thuy, A. Maurice, N. Q. Liem, and P. Reiss, “Europium doped In(Zn)/ZnS colloidal quantum dots,” *Dalton Trans.* **42**, 12606–12610 (2013).
- <sup>45</sup>K. E. Johnson and J. N. Sandoe, “An interpretation of the spectra of bivalent rare-earth ions in crystals,” *J. Chem. Soc. A* **1969**, 1694–1697 (1969).
- <sup>46</sup>R. Reisfeld and A. Glasner, “Absorption and fluorescence spectra of Eu<sup>2+</sup> in alkali halide crystals,” *J. Opt. Soc. Am.* **54**(3), 331–333 (1964).
- <sup>47</sup>N. K. Kumawat, X.-K. Liu, D. Kabra, and F. Gao, “Blue perovskite light-emitting diodes: Progress, challenges and future directions,” *Nanoscale* **11**(5), 2109–2120 (2019).
- <sup>48</sup>M. Protiere and P. Reiss, “Amine-induced growth of an In<sub>2</sub>O<sub>3</sub> shell on colloidal InP nanocrystals,” *Chem. Commun.* **2007**(23), 2417–2419 (2007).
- <sup>49</sup>A. Cros-Gagneux, F. Delpéch, C. Nayral, A. Cornejo, Y. Coppel, and B. Chaudret, “Surface chemistry of InP quantum dots: A comprehensive study,” *J. Am. Chem. Soc.* **132**(51), 18147–18157 (2010).
- <sup>50</sup>J. E. Huheey, E. A. Keiter, and R. L. Keiter, *Inorganic Chemistry: Principles of Structure and Reactivity*, 4th ed. (Harper Collins College Publishers, New York, 1993).
- <sup>51</sup>M. Imran, P. Ijaz, D. Baranov, L. Goldoni, U. Petralanda, Q. Akkerman, A. L. Abdelhady, M. Prato, P. Bianchini, I. Infante, and L. Manna, “Shape-pure, nearly monodispersed CsPbBr<sub>3</sub> nanocubes prepared using secondary aliphatic amines,” *Nano Lett.* **18**(12), 7822–7831 (2018).
- <sup>52</sup>S. Thapa, K. Bhardwaj, S. Basel, S. Pradhan, C. J. Eling, A. M. Adawi, J.-S. G. Bouillard, G. J. Stasiuk, P. Reiss, A. Pariyar, and S. Tamang, “Long-term ambient air-stable cubic CsPbBr<sub>3</sub> perovskite quantum dots using molecular bromine,” *Nanoscale Adv.* **1**, 3388–3391 (2019).